THE JOURNAL OF BIOLOGICAL CHEMISTRY VOL. 289, NO. 7, pp. 4432–4443, February 14, 2014

Structure-guided Development of Specific Pyruvate Dehydrogenase Kinase Inhibitors Targeting the ATP-binding Pocket*[S]

Received for publication, November 12, 2013, and in revised form, December 13, 2013 Published, JBC Papers in Press, December 19, 2013, DOI 10.1074/jbc.M113.533885

Shih-Chia Tso[‡1], Xiangbing Qi[‡1], Wen-Jun Gui[‡], Cheng-Yang Wu[‡], Jacinta L. Chuang[‡], Ingrid Wernstedt-Asterholm[§2], Lorraine K. Morlock[‡], Kyle R. Owens[‡], Philipp E. Scherer[§], Noelle S. Williams[‡], Uttam K. Tambar[‡3], R. Max Wynn[‡§], and David T. Chuang[‡§4]

From the Departments of [‡]Biochemistry and [§]Internal Medicine, University of Texas Southwestern Medical Center, Dallas, Texas 75390

Background: Up-regulated pyruvate dehydrogenase kinase isoforms (PDKs) are associated with impaired glucose homeostasis in diabetes.
Results: Novel PDK inhibitors were developed using structure-based design, which improves glucose tolerance with reduced hepatic steatosis in diet-induced obese mice.
Conclusion: Obesity phenotypes are effectively treated by chemical intervention with PDK inhibitors.
Significance: PDKs are potential drug targets for obesity and type 2 diabetes.

Pyruvate dehydrogenase kinase isoforms (PDKs 1–4) negatively regulate activity of the mitochondrial pyruvate dehydrogenase complex by reversible phosphorylation. PDK isoforms are up-regulated in obesity, diabetes, heart failure, and cancer and are potential therapeutic targets for these important human diseases. Here, we employed a structure-guided design to convert a known Hsp90 inhibitor to a series of highly specific PDK inhibitors, based on structural conservation in the ATP-binding pocket. The key step involved the substitution of a carbonyl group in the parent compound with a sulfonyl in the PDK inhibitors. The final compound of this series, 2-[(2,4-dihydroxyphenyl)sulfonyl]isoindoline-4,6-diol, designated PS10, inhibits all four PDK isoforms with IC_{50} = 0.8 μM for PDK2. The administration of PS10 (70 mg/kg) to diet-induced obese mice significantly augments pyruvate dehydrogenase complex activity with reduced phosphorylation in different tissues. Prolonged PS10 treatments result in improved glucose tolerance and notably lessened hepatic steatosis in the mouse model. The results support the pharmacological approach of targeting PDK to control both glucose and fat levels in obesity and type 2 diabetes.

The mitochondrial pyruvate dehydrogenase complex (PDC)[5] catalyzes the oxidative decarboxylation of pyruvate to give rise to acetyl-CoA and is the gate-keeping enzyme linking glycolysis and the Krebs cycle. The mammalian PDC is a 9.5 million-dalton protein machine organized about a 60-meric core consisting of dihydrolipoyl transacetylase (E2) and the E3-binding protein (E3BP), to which multiple copies of pyruvate dehydrogenase (E1) and dihydrolipoyl transacetylase (E2), dihydrolipoamide dehydrogenase (E3), as well as isoforms of pyruvate dehydrogenase kinase (PDKs 1–4) and pyruvate dehydrogenase phosphatase (PDPs 1–2) are attached through ionic interactions (1). Because of its strategic location, the regulation of PDC activity is critical for glucose homeostasis and fuel selection in the glucose-fatty acid cycle (2). The mammalian PDC is acutely regulated by reversible phosphorylation (3). The phosphorylation of PDC by PDK results in inactivation, and dephosphorylation by PDP restores PDC activity. When glucose levels are low during fasting, PDC is highly phosphorylated and inactive, so as to preserve the substrates (pyruvate, lactate, and alanine) for gluconeogenesis (2).

The PDKs are potential therapeutic targets because of increased PDK expression in disease states such as diabetes, cancer, and heart failure. PDK4, but not PDK2, is drastically induced in muscle and heart in streptozotocin-induced diabetes (4), obesity (5), and type 2 diabetes (6), which attenuates PDC activity leading to reduced glucose oxidation. The accumulated evidence has established that the up-regulation of PDK4 is mediated through the peroxisome proliferator-activated receptor α-FOXO3α-PGC-1α complex (4). The PDK2/

* This work was supported, in whole or in part, by National Institutes of Health Grants DK62306, DK26758, DK55758, DK92921, and GM102604. This work was also supported by Grants I-1286 and I-1748 from the Welch Foundation and the Sloan Research Fellowship.
[S] This article contains supplemental text.
The atomic coordinates and structure factors (codes 4MP2, 4MP7, 4MPC, 4MPE, and 4MPN) have been deposited in the Protein Data Bank (http://wwpdb.org/).
[1] Both authors contributed equally to this work.
[2] Supported by a fellowship from the Throne-Host Foundation, the Swedish Research Council Grant 2006-3931, and from VINNOVA (Marie Curie Qualification).
[3] To whom correspondence may be addressed. E-mail: Uttam.Tambar@UTSouthwestern.edu.
[4] To whom correspondence may be addressed. E-mail: David.Chuang@UTSouthwestern.edu.

[5] The abbreviations used are: PDC, pyruvate dehydrogenase complex; E1, pyruvate dehydrogenase; E2, dihydrolipoyl transacetylase; E3, dihydrolipoamide dehydrogenase; E3BP, E3-binding protein; PDK, pyruvate dehydrogenase kinase; PDP, pyruvate dehydrogenase phosphatase; PGC-1, peroxisome proliferator-activated receptor-γ coactivator-1; DCA, dichloroacetate; Hsp90, heat shock protein 90; DIO, diet-induced obese; ITC, isothermal titration calorimetry; OCT, optimal cutting temperature compound.

PDK4 double knock-out mice fed a high fat diet show marked improvements in glucose tolerance and insulin sensitivity over wild-type mice on the same diet (7). The expression of PDK1 (8–10), PDK2 (11), and PDK3 (12) is significantly elevated in certain cancers. Tyrosine phosphorylation of PDK1 with increased kinase activity is essential for tumor cell proliferation and hypoxia (13). Inhibition of PDK activity with dichloroacetate (DCA) or siRNA promotes apoptosis in cancer cells and impedes tumor growth (14).

The classic PDK inhibitor DCA, an analog of the PDC substrate pyruvate, has been used since early 1970 to inhibit PDK activity and increase PDC flux, with concomitant reduction in glucose levels in animals (15). DCA exerts its inhibitory effects by binding to an allosteric site in the N-terminal domain of PDK isoforms (16, 17). However, DCA is a nonspecific low potency PDK inhibitor and requires high doses for its therapeutic effects (18), which leads to peripheral neurological toxicity and tumor growth (19). (*R*)-Lipoic acid in millimolar concentrations abates PDK activity *in vitro* (20), but its function as a PDK inhibitor *in vivo* is uncertain. Phenylbutyrate enhances PDC activity *in vitro* and *in vivo* (21), but the compound is a modest PDK inhibitor (K_i = 0.3 mM) with multiple targets and diverse clinical applications (22). Dihydrolipoamide mimetics, including AZD7545 (23) and secondary amides of SDZ048-619 (24), have also been developed. This family of compounds inhibits PDK2 activity by impeding PDK binding to the E2/E3BP core of PDC (25). Paradoxically, these dihydrolipoamide mimetics strongly stimulates PDC core-free PDK4 activity *in vitro*, which precludes these compounds as *bona fide* PDK inhibitors (26). To date, there have been no effective PDK inhibitors for novel therapeutic approaches to cancer, obesity, and type 2 diabetes as well as heart disease.

Mitochondrial PDK isoforms are members of the GHKL ATPase/kinase superfamily that includes DNA *g*yrase B, heat-shock protein 90 (Hsp90), histidine kinases CheA and EnvZ, as well as the DNA-repair enzyme MutL (27). Members of this superfamily share four conserved motifs (N-, G1-, G2-, and G3-boxes) that build a unique Bergerat ATP-binding fold consisting of a four-stranded mixed β-sheet and three α-helices and is located in the C-terminal domains of PDK isoforms (28, 29). This signature fold also contains a unique structural element known as the "ATP lid," whose conformational change is coupled to ATP hydrolysis and protein-protein interactions (29).

In this study, we sought to develop robust PDK inhibitors that can be used to improve glucose metabolism and correct metabolic dysfunction *in vivo*. Based on the unique structural features present in the ATP-binding pocket of PDK2, a single functional group change was made in a known Hsp90 inhibitor that binds to the corresponding pocket of the latter protein (30, 31) from the GHKL family. This approach efficiently converted the Hsp90 inhibitor to a highly specific inhibitor for all PDK isoforms. The final PDK inhibitors of this series robustly augments PDC activity with reduced phosphorylation in tissues, which leads to improved glucose tolerance and reduced hepatic steatosis in diet-induced obese (DIO) mice. These findings demonstrate the utility of structure-based inhibitor design and support the pharmacological approach of targeting PDK to control glucose and fat levels in obesity and type 2 diabetes.

EXPERIMENTAL PROCEDURES

Chemicals—All reagents and chemicals were obtained from Sigma unless otherwise indicated. Synthesis of novel PDK inhibitors PA1, PA7, PS2, PS8, and PS10 were described in the supplemental material.

Proteins—Recombinant human PDK2 was expressed and purified as an N-terminal His_6-tagged SUMO fusion protein with a tobacco etch virus protease cleavage site in front of the N-terminal PDK2 sequence (26), and it was used directly for the activity assay and binding affinity analyses. For crystallization, the protein was subjected to tobacco etch virus protease digestion, and the untagged PDK2 protein was purified on a Superdex 200 column in 20 mM Tris-HCl, pH 8.0, 150 mM NaCl, and 5 mM DTT. The purified protein was concentrated to 35–40 mg/ml and stored at −80 °C in small aliquots. Recombinant human PDK1, PDK3, and PDK4 were expressed and purified as described previously (26).

To express the N-terminal domain (residue 1–236) of human Hsp90, the first strand cDNA was synthesized with the human total RNA as template using the Omniscript Reverse Transcriptase from Qiagen (Gaithersburg, MD). The sequence encoding the N-terminal domain was amplified and cloned into the pSUMO expression vector (LifeSensors, Malvern, PA). The fusion protein of His_6-tagged SUMO-Hsp90 N-terminal domain was expressed in *Escherichia coli* BL21 cells and purified with nickel-nitrilotriacetic acid resin (Qiagen) and on a Superdex-200 column in 20 mM Tris-HCl, pH 7.5, and 500 mM NaCl.

Assay for Inhibition of PDK Activity—To determine the IC_{50} for PDK inhibitors, a mixture containing 0.05–0.2 μM PDK, 6 μM E1, with or without 0.5 μM of the PDC core E2/E3BP, and various amounts of inhibitor was incubated at 25 °C for 10 min in a buffer of 20 mM Tris-Cl, pH 7.5, 10 mM KCl, 5 mM $MgCl_2$, 2 mM DTT, 0.02% (v/v) Tween 20, and 0.1 mg/ml bovine serum albumin before the addition of 50 μM ATP to initiate the reaction. All inhibition titrations were performed at 10 dose points ranging from 31.6 to 1 mM in a 3.162-fold dilution series, with each inhibitor concentration tested in duplicate. The remaining steps were described previously (26). IC_{50} values were obtained by the curve fitting of inhibition isotherms using Prism 6 (GraphPad Software, Inc.).

The kinase profiling of PS8 on 21 human protein kinases was performed at Reaction Biology Corp. (Malvern, PA). IC_{50} values were determined by a 10-dose titration of PS8 from 15 nM to 300 μM in the presence of 10 μM ATP. Each protein kinase was also tested against its known inhibitor as a positive control.

Isothermal Titration Calorimetry (ITC)—The PDK2 or Hsp90 N-terminal domain protein was dialyzed against 1 liter of the dialysis buffer containing 50 mM Tris-Cl, pH 7.5, 50 mM KCl, 1 mM $MgCl_2$, and 0.5 mM β-mercaptoethanol. Known or novel PDK inhibitor solutions (150–1500 μM) were placed in the titration syringe and injected in 8-μl increments into the reaction cell containing 1.4 ml of 18–70 μM PDK2 or Hsp90 N-terminal domain at 15 °C in a VP-ITC microcalorimeter (GE Healthcare). All of the ITC data were initially analyzed by the

NITPIC program (32) to construct the baseline, followed by curve-fitting in Origin 7 to obtain binding parameters. The concentrations of PDK2 and Hsp90 N-terminal domain proteins were determined by measuring A_{280} and using calculated molar extinction coefficients (M^{-1} cm^{-1}) of 49,530 and 18,910, respectively.

Crystallization of PDK2 and PDK2-Inhibitor Complexes—Crystals of human PDK2 were obtained by the hanging-drop vapor-diffusion method. Two μl of protein solution was mixed with 2 μl of the well solution (0.9 M ammonium tartrate, 0.1 M sodium acetate, pH 4.6) and kept in a 20 °C incubator. Crystals were developed in 1 week and reached the size of 500 μm in 2 weeks. Mature crystals were transferred to a fresh soaking solution (0.75 M ammonium tartrate, 0.1 M sodium acetate, pH 4.6, and 5% glycerol with various indicated inhibitors). After overnight incubation, crystals were serially transferred to a cryosolution containing 20% glycerol and snap-frozen in liquid nitrogen.

Structure Determination and Refinements—All x-ray diffraction data for PDK2 and PDK2-inhibitor complexes were collected at beamline 19-ID at the Advanced Photon Source, Argonne National Laboratories. Diffraction data for each PDK2-inhibitor complex were collected from a single crystal. All crystals share the same space group of $I4_122$, and the highest resolution of diffraction ranged from 1.70 to 1.95 Å. The molecular replacement, structure modeling, and refinement were performed as described previously (33). The crystal structure of inhibitor-free human PDK (PDB code 2BTZ) was used as the search model.

Pharmacokinetic Studies—Twenty one male C57BL/6J mice were dosed i.p. with 70 mg/kg PS-10, 0.2 ml/mouse formulated as 10% DMSO, 20% water, 70% of 25% (2-hydroxypropyl)-β-cyclodextrin for determination of PS-10 PK. Twenty one female CD-1 mice were dosed i.p. with 20 mg/kg PS-8, 0.2 ml/mouse formulated as 5% ethanol and 95% of 0.1 M sodium bicarbonate, pH 9.0, for determination of PS-8 PK. Animals ($n = 3$) were sacrificed, and whole blood was harvested for each time point. Plasma was processed from whole blood by centrifugation of the acidified citrate dextrose-treated blood for 10 min at 10,000 rpm in a standard centrifuge. The analytical processing of blood samples and pharmacokinetics studies using LC/MS/MS were as described previously with LC/MS/MS methods optimized for detection of PS-10 and PS-8 (33).

Treatments of Mice with PDK Inhibitors—Six- to eight-week-old C57BL/6J male mice were obtained from the local campus breeding colony at University of Texas Southwestern Medical Center (Dallas, TX) and randomized into two groups, vehicle- and PS10-treated. Prior to the treatment, mice were fed with a 60% high fat diet, which contained 32% saturated and 68% unsaturated fat (catalog no. D12492, Research Diet Inc., New Brunswick, NJ), for 8–10 weeks to produce DIO animals. PS-10 was dissolved in 100% DMSO and then diluted to make a 10% DMSO aqueous solution containing 17.5% (w/v) (2-hydroxypropyl)-β-cyclodextrin for delivery. Animals were dosed at mid-day by i.p. injections at 70 mg/kg using a 1-ml syringe and a 30-gauge needle. The length of the treatment is indicated in each experiment. At 10 h after the last injection, animals were euthanized using carbon dioxide asphyxiation followed by cervical dislocation and dissection. Blood was harvested by cardiac puncture and stored on ice. Acidified citrate dextrose was used as an anticoagulant. Immediately after blood collection, heart, liver, kidneys, and both hind leg quadriceps muscles were removed and snap-frozen in liquid nitrogen. Average ischemia time before organ harvest was about 2–3 min. Blood was centrifuged in an Eppendorf 5415R refrigerated microcentrifuge at 9300 $\times$ *g* for 5 min to isolate plasma, which was subsequently stored at −80 °C.

Assay for PDC Activity in Mouse Tissues—Liquid nitrogen-stored tissue samples were removed and thawed on ice. Individual kidneys (200–250 mg), hearts (200–300 mg), muscle (200–300 mg), and liver (250–400 mg) tissues samples were manually homogenized in an ice-chilled glass homogenizer containing 1 ml of the homogenization buffer. The homogenization buffer contained 30 mM KP_i, pH 7.5, 3 mM EDTA, 5 mM DTT, 1 mM benzamidine, 3% fetal bovine serum, 5% Triton X-100, and 1 mM leupeptin. Samples were transferred to ice-cold 10-ml polycarbonate tubes and spun in an ultracentrifuge at 25,000 $\times$ *g* for 10 min to pellet cell and tissue debris. Supernatants were removed and stored on ice until diluted (1:3 for muscle, 1:5 for liver, and 1:20 for kidneys and heart tissues) with a dilution buffer containing 50 mM HEPES, pH 7.5, 1.0 mM DTT, 0.1% Triton X-100, 5 mM DCA, 50 mM NaF, 3% fetal bovine serum, and 1 mM leupeptin. The diluted samples (50 μl) were placed in each well of a 24-well plate containing 310 μl of the reaction mixture. A micro-bridge (Hampton Research) was pre-set into each well holding one piece of filter wick pre-soaked with 2 M NaOH. The reaction mixture contained 30 mM KP_i, pH 7.5, 0.4 mM CoA, 3 mM NAD^+, 5% fetal bovine serum, 2 mM thiamine diphosphate, 2 mM $MgCl_2$, and 65 μg of recombinant human E3. [1-^{14}C]Pyruvate (PerkinElmer Life Sciences) was added to each well to initiate the reaction, with the wells sealed with a clear Mylar adhesive film. The assay plates were incubated at 37 °C for 10 min. Fifty μl of a 20% TCA solution was added to each well to stop the reaction. Assay plates were incubated further at 37 °C for 45 min. $^{14}CO_2$ trapped on 2 M NaOH soaked filter wicks were counted in a liquid scintillation counter. Total protein concentrations in the samples were determined by using BCA protein assay kit (ThermoFisher Scientific, Rockford, IL).

Western Blotting—SDS-polyacrylamide gels were run using 15–20 μg of protein lysate per lane. Western blots were transferred to PVDF membranes for 2 h at 200 mV. PVDF membranes were blocked with 5% nonfat dried milk and then probed using polyclonal antibodies to pyruvate dehydrogenase/decarboxylase E1α and to phosphorylate E1α (pE1α). The E1α antibody was obtained from MitoSciences/Abcam (Cambridge, MA). Antibodies against the phosphorylated serine (Ser(P)-293) residue of the E1α subunit were purchased from EMD Millipore/Calbiochem. One milliliter of Luminata Forte Western HRP (Millipore Corp., Billerica, MA) substrate reagent was pipetted across the membrane for signal detection in a FluorChem E system (Cell Biosciences, Santa Clara, CA).

Glucose Tolerance Test—Mice were fasted for 6 h after compound treatment. Ten hours after compound administration, 1.5 g/kg glucose was delivered intraperitoneally to mice. Tail vein serum samples were collected immediately before and 15,

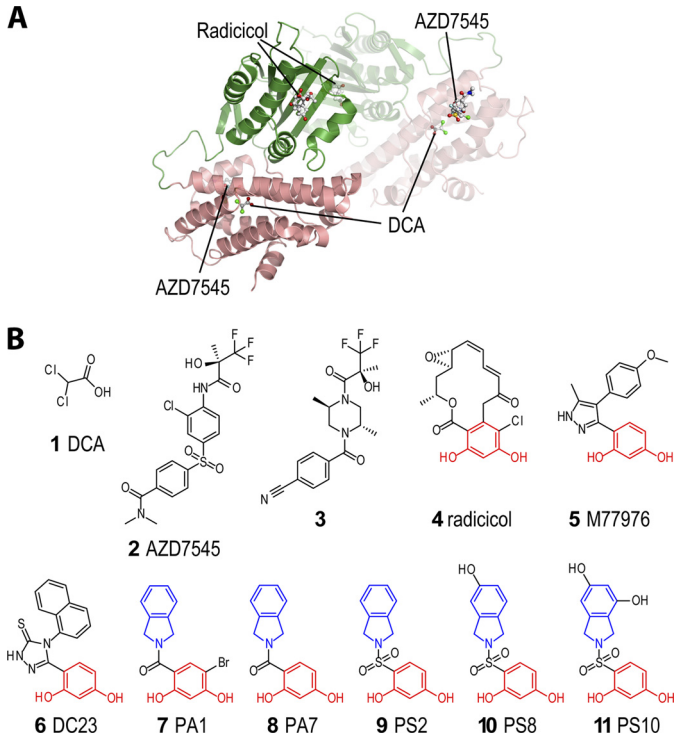

FIGURE 1. **Structure of PDK2 and known and novel inhibitors.** *A*, PDK dimer showing AZD7545 and dichloroacetate-binding sites in N-terminal domain (*pink*) and radicicol bound to the ATP-binding pocket in the C-terminal domain (*green*). *B*, chemical structures of known PDK inhibitors as follows: DCA, AZD7545, compound **3**, radicicol, and M77976; and novel PDK inhibitors as follows: DC23, PA1, PA7, PS2, PS8, and PS10. The resorcinol ring is indicated in *red*, and isoindoline moiety is in *blue*.

30, 60, and 120 min after the glucose challenge. The glucose levels in serum samples were determined by a glucose meter.

Blood Biochemistry—Glucose levels were determined with glucose (Sigma). The levels of lactate, cholesterol, and triglyceride were measured by Vitros 250 blood chemistry analyzer (Johnson & Johnson Inc.) in the Metabolic Phenotyping Core at University of Texas Southwestern Medical Center.

Histochemistry of the Liver—Histological examination of the liver was performed in the institutional immunohistochemistry laboratory. Liver tissue was dissected, grossly trimmed, and then fixed by immersion for 48 h in 4% formalin/PBS (4% formic acid, 137 mM NaCl, 2.7 mM KCl, and 10 mM phosphate buffer, pH 7.5) at 4 °C. Liver samples were then transferred to 10% (w/v) sucrose in PBS and incubated at 4 °C for 24 h. Tissues were incubated in 18% sucrose in PBS at 4 °C for 24 h. Finally, samples were transferred to a fresh 18% sucrose solution and embedded in optimal cutting temperature compound, cryosectioned, and stained with Oil Red O.

Statistical Analysis—Data are shown as mean ± S.D. Prism 6.0 (GraphPad Inc.) was used to perform the two-tailed Student's *t* test for comparison between groups and nonlinear regression to fit inhibition curves. *, $p < 0.05$ is considered significant; **, $p < 0.01$; ***, $p < 0.001$.

RESULTS

In Vitro Potencies of Known PDK Inhibitors—As shown in Fig. 1*A*, PDK is a homodimer with each monomer consisting of an N-terminal regulatory domain (*pink*) and a C-terminal nucleotide-binding domain (*green*). The active-site cleft is formed between the side walls of these two domains. Based on the PDK inhibitor structures, the known PDK inhibitors DCA (IC_{50} = 290 μM) (34) and AZD7545 (IC_{50} = 87 nM-600 nM) bind to the pyruvate-binding site and the lipoyl-binding pocket, respectively, in the N-terminal domain of PDK (16). The SDZ048-619 derivative, (+)-1-*N*-[2,5-(*SR*)-dimethyl-4-*N*-(4-cyanobenzoyl)piperazine]-(*R*)-3,3,3-trifluoro-2-hydroxy-2-methylpropanamide (compound **3**), with IC_{50} = 16 nM, is an analog of AZD7545, and it likely also binds to the lipoyl-binding pocket (24). All the above compounds are allosteric PDK inhibitors, because their binding sites in the N-terminal domain are distant from the active-site cleft. In contrast, antibiotic radicicol (Fig. 1*B*) (IC_{50} = 230–400 μM) (16) and M77976 (IC_{50} = 648 μM) (35) dock to the ATP-binding pocket in the C-terminal domains of PDK3 and PDK4, respectively, and are ATP-competitive inhibitors. Except for AZD7545 and compound **3**, the above known PDK inhibitors show IC_{50} in the sub-molar range. PDKs and Hsp90 of the GHKL family show conserved chain folds in the ATP-binding pocket (27); however, radicicol shows a far better binding affinity for Hsp90 (K_d = 46.3 nM) than PDK2 (K_d = 18,600 nM). Similarly, M77976 also inhibits Hsp90 significantly better than PDK4, with an IC_{50} of 4.4 μM for Hsp90 (36) compared with 648 μM for PDK4 (see above).

TABLE 1
IC_{50} values and dissociation constants of known and novel PDK inhibitors

PDK activity was assayed with increasing concentrations (31.6 nM to 1 mM) of the inhibitor as described under "Experimental Procedures." IC_{50} values were obtained by the curve fitting of inhibition isotherms using program Prism 6 (GraphPad software, Inc.). Dissociation constants (K_d) were determined by ITC as also described under "Experimental Procedures."

Compound	IC_{50}, μM for PDK2	IC_{50}, μM for PDK4	K_d, nM for PDK2	K_d, nM for Hsp90
DCA[a]	183	80.0		
Radicicol[a]	77.8		18,600 ± 3200	46.3 ± 7.2
DC23	3.82	0.28	6760 ± 2040	25.0 ± 10.1
PA1	6.78	1.86	3570 ± 560	6.0 ± 2.6
PA7	5.68	1.05	1827 ± 179	27.3 ± 2.5
PS2	2.11	2.20	711 ± 33	50,900 ± 9200
PS8	1.07	1.10	426 ± 32	60,100 ± 1300
PS10	0.80	0.76	239 ± 16	47,000 ± 5200

[a] Known PDK inhibitor.

Single Functional Group Substitution Converts an Hsp90 Inhibitor to a PDK-specific Inhibitor—Compound DC23 identified by high throughput screens performed in this laboratory shows a good potency for inhibition of both PDK4 (IC_{50} = 0.8 μM) and PDK2 (IC_{50} = 3.82 μM) (Table 1). However, similar to M77976, DC23 is also an inhibitor for Hsp90 with IC_{50} = 0.3 μM (37). DC23 shows a much higher binding affinity for Hsp90 than PDK2 with K_d values of 25 and 6,760 nM, respectively (Table 1). Radicicol, M77976, and DC23 share a common resorcinol moiety (highlighted in *red*) in their respective structures (Fig. 1*B*). In light of the significant conservation in the ATP-binding pocket between PDKs and Hsp90, compounds PA1 and PA7, which were reported as Hsp90 inhibitors (30, 31), were synthesized. PA1 inhibits both PDK2 (IC_{50} = 6.78 μM) and PDK4 (IC_{50} = 1.86 μM) (Table 1). Similarly, PA7 shows IC_{50} values of 5.68 and 1.05 μM for PDK2 and PDK4, respectively. Both PA1 and PA7 contain a carbonyl group sandwiched between an isoindoline ring (Fig. 1*B*, highlighted in *blue*) and a

TABLE 2
Crystallographic data collection and refinement statistics (molecular replacement)

	PDK2+PA1	PDK2+PA7	PDK2+PS2	PDK2+PS8	PDK2+PS10
PDB code	4MP2	4MP7	4MPC	4MPE	4MPN
Data collection					
Space group	$I4_122$, 1 molecular per asymmetric unit, ~70% solvent content				
Cell dimensions					
a, *b*	110.32 Å	110.01 Å	110.63 Å	110.42 Å	110.62 Å
c	229.52 Å	227.74 Å	228.57 Å	228.62 Å	228.74 Å
α, β, γ	$\alpha = \beta = \gamma = 90°$	$\alpha = \beta = \gamma = 90°$	$\alpha = \beta = \gamma = 90°$	$\alpha = \beta = \gamma = 90°$	$\alpha = \beta = \gamma = 90°$
Resolution	50 to 1.75 Å (1.78 to 1.75 Å)[a]	50 to 1.80 Å (1.83 to 1.80 Å)	50 to 1.70 Å (1.73 to 1.70 Å)	50 to 1.95 Å (1.98 to 1.95 Å)	50 to 1.75 Å (1.78 to 1.75 Å)
R_{merge}	4.6 (71.7)	6.7 (91.1)	4.9 (84.5)	6.9 (82.7)	5.0 (75.6)
$I/\sigma I$	40.3 (3.1)	30.9 (2.6)	42.1 (2.1)	29.8 (2.4)	53.3 (3.5)
Completeness	99.1% (100.0%)	99.9% (100.0%)	99.5% (100.0%)	99.9% (100.0%)	99.9% (100.0%)
Redundancy	7.9 (8.0)	10.3 (10.3)	7.8 (7.1)	9.3 (9.4)	14.1 (14.2)
Refinement					
Resolution	1.75 Å	1.80 Å	1.70 Å	1.95 Å	1.75 Å
No. of reflections	70,461	64,713	77,555	51,386	118,280
R_{work}/R_{free}	20.4/21.9%	19.1/20.5%	19.9/21.8%	19.2/20.4%	18.7/20.2%
No. of atoms					
Protein	3000	2965	3040	2958	3011
Inhibitor	20	19	20	21	22
Tartrate	10	10	10	10	10
Water	212	213	197	184	179
B-factors					
Protein	36.4	35.3	36.4	41.2	27.0
Inhibitor	47.7	22.8	24.4	29.7	14.7
Tartrate	55.5	53.6	52.9	62.0	48.8
Water	44.0	41.9	41.5	44.3	29.2
Root mean square deviations					
Bond lengths	0.006 Å	0.006 Å	0.006 Å	0.007 Å	0.007 Å
Bond angles	1.093°	1.018°	1.099°	1.037°	1.043°

[a] Values in parentheses are for highest resolution shell.

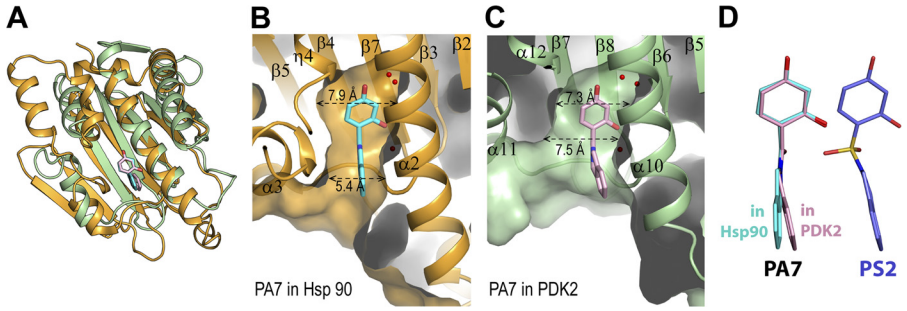

FIGURE 2. **Comparison of inhibitor-binding pockets in PDK2 and Hsp90.** *A*, superimposition of the C-terminal domain of PDK2 (*green*) harboring PA7 (*pink*) with the N-terminal domain of Hsp90 (*orange*) with bound PA7 (*cyan*). *B*, PA7 in Hsp90. *C*, PA7 in PDK2. *D*, superimposition of Hsp90-bound (*cyan*) and PDK2-bound PA7 (*pink*) (*left*), and the structure of PDK2-bound PS2 (*right*).

resorcinol moiety (highlighted in *red*). As expected, PA1 preferentially binds to Hsp90 (K_d = 9.0 nM) over PDK2 (K_d = 3,570 nM). PA7, with the 5-bromo group removed from the resorcinol ring, is also a far more potent ligand for Hsp90 (K_d = 27.3 nM) than PDK2 (K_d = 1,827 nM). Remarkably, a single substitution of the carbonyl group in PA7 with a sulfonyl group practically converts the potent Hsp90 inhibitor PA7 to a PDK-specific inhibitor in PS2. The IC_{50} is 2.11 μM for PDK2; more significantly, the K_d values are 711 nM for PDK2 and 50,900 nM for Hsp90. Based on these new K_d values, the change from the carbonyl group in PA7 to the sulfonyl group as in PS2 represents 4,791-fold shift in binding affinities in favor of the PDK2. The addition of the 5-hydroxyl group to the isoindoline ring in PS8 results in improved IC_{50} values for both PDK2 (1.07 μM) and PDK4 (1.10 μM) (Table 1). The relative binding affinities for PDK2 (K_d = 426 nM) and Hsp90 (K_d = 60,100 nM) become more favorable for PDK2. The introduction of a second hydroxyl group to the isoindoline ring generates PS10 with significantly better IC_{50} and K_d values than those for PS8 for PDK2 and PDK4. The K_d value of 239 nM for PS10 binding to PDK2 is the lowest among the ATP-competitive PDK inhibitors.

Structures of PDK2-Inhibitor Complexes Reveal a Distinct Ligand-binding Mode—PDK2 crystals were soaked with 0.25 to 0.5 mM concentrations of various PDK inhibitors. Crystals of PDK2-inhibitor complexes diffracted to 1.70–1.95-Å resolutions. All residues were in the most favorable and allowed regions of the Ramachandran plot. The final models show excellent geometry and residual statistics (Table 2).

Fig. 2*A* shows a high degree of conservation in the nucleotide-binding domain between PDK2 and Hsp90, when the PDK2-PA7 structure (in *green*, this study) is superimposed with the published Hsp90-PA7 structure (in *orange*) (30). However, the size and contour of the ATP-binding pocket in Hsp90 significantly differ from those of the corresponding pocket in PDK2. In Hsp90, the ATP-binding pocket shows a narrow opening of 5.2 Å leading to a deep tunnel-like surface (Fig. 2*B*).

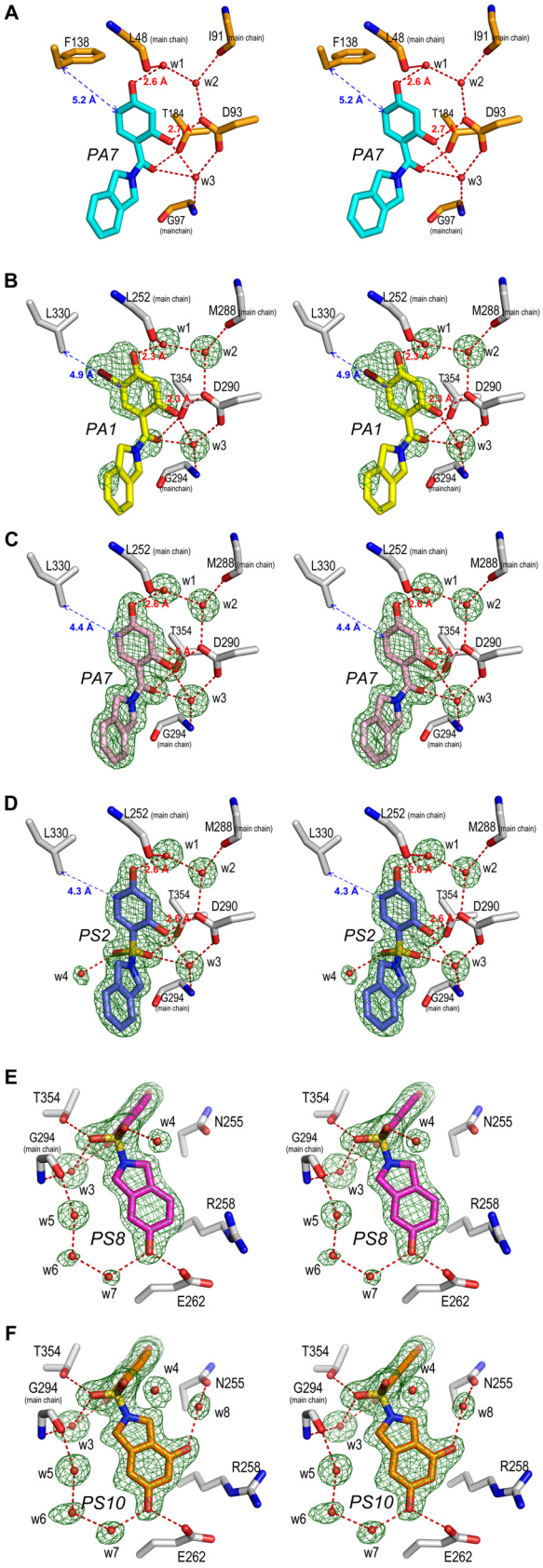

FIGURE 3. **Stereo views of inhibitor-binding pockets in PDK2 and Hsp90.** *A*, Hsp90-PA7 structure (30). *B*, PDK2-PA1 structure with $F_o - F_c$ density map (*green mesh*) contoured to 4 σ. *C*, PDK2-PA7 structure contoured to 4 σ. *D*, PDK2-PS2 structure contoured to 4 σ. *E*, PDK2-PS8 structure contoured to 3 σ. *F*, PDK2-PS10 structure contoured to 3 σ. *w*, ordered water molecule.

By comparison, the ATP-binding pocket in PDK2 shows a wider opening of 7.5 Å with a shallow cavity (Fig. 2*C*). These differences form the basis for the structure-based design of PDK-specific inhibitors. PA7 binds to the ATP-binding pocket of Hsp90 with the isoindoline ring in a planar conformation (Fig. 2*B*). In contrast, the same ring in PDK2-bound PA7 is tilted toward the α10 helix (Fig. 2*C*). The different conformations in the isoindoline ring become apparent when the Hsp90-bound PA7 structure is superimposed with the PDK2-bound PA7 structure (Fig. 2*D*). The more relaxed planar orientation of the isoindoline ring in Hsp90 explains, in part, the drastically higher binding affinity of Hsp90 for PA7 than PDK2 (Table 1). In PDK2, PA7 interacts with conserved Leu-252 in the N box, Asp-290 and Gly-294 in the G1 box, and Thr-354 in the G3 box (Fig. 3*C*). Equivalent contacts are observed in the Hsp90-PA7 structure (Fig. 3*A*). Similar interactions are also present in the PDK2-PA1 and PS2 structures (Fig. 3, *B* and *D*). The substitution of a carbonyl group in PA7 with a sulfonyl group in PS2 retains the favorable position of the isoindoline ring in PDK2-bound PS2 (Fig. 2*D*). However, the tetrahedral bond angles of the sulfonyl group in PS2, when bound to Hsp90, can conceivably cause the isoindoline ring to clash with the α2 helix in Hsp90, resulting in the markedly reduced affinity of Hsp90 for PS2 compared with PA7 (Table 1). The incorporation of the 5-OH group to the isoindoline ring in PS8 promotes interactions of the hydroxyl group with Glu-262 (Fig. 3*E*), which is unique for PDK isoforms, making PS8 a better PDK inhibitor than PS2 (Table 1). The presence of two OH groups in the isoindoline ring in PS10 permits the second OH group to contact, through a water molecule, Asn-255 of the N box while maintaining the contact with Glu-262 (Fig. 3*F*). The additional interactions with Asn-255 through the second OH group likely foster the better IC_{50} and K_d values of PS10 compared with PS8.

The above structures of the PDK2-inhibitor complexes establish that all novel inhibitors from this study (PA1, PA7, PS2, PS8, and PS10) occupy the adenine region of ATP-binding pocket in PDK2. These synthetic inhibitors do not extend into the space normally accommodated by the phosphoryl groups of ATP, *i.e.* the phosphate region. Recent studies have shown that K^+ ions, which coordinate with the α-phosphoryl group of bound ATP in the ATP-binding pocket, are critical for high affinity nucleotide binding to PDK2 (38, 39). The presence or absence of 50 mM KCl has no effect on the binding affinity (K_d) of PS10 for PDK2 measured by ITC (data not shown). The results are consistent with the lack of PS10 interactions with residues in the phosphate region of the ATP-binding pocket.

PS Series Inhibitors Show Favorable Binding Enthalpies for PDK2—The binding of PDK inhibitors to PDK2 or Hsp90 was measured by ITC. The fitting of binding isotherms (Fig. 4*A*) showed a distinctly higher affinity of PS10 for PDK2 (K_d = 239 nM) than for Hsp90 (K_d = 47,000 nM). The binding enthalpy (ΔH in kcal/mol) of PS10 for Hsp90 is also shown much smaller than that for PDK2 (Fig. 4*A*). The development of compounds from PA1 toward PS10 on the same chemical scaffold was accompanied by the steadily more favorable (*i.e.* more negative) thermodynamic signatures in terms of binding enthalpies (ΔH) and Gibbs binding energies (ΔG), when titrated into PDK2, although the term of binding entropies ($-T\Delta S$) becomes less

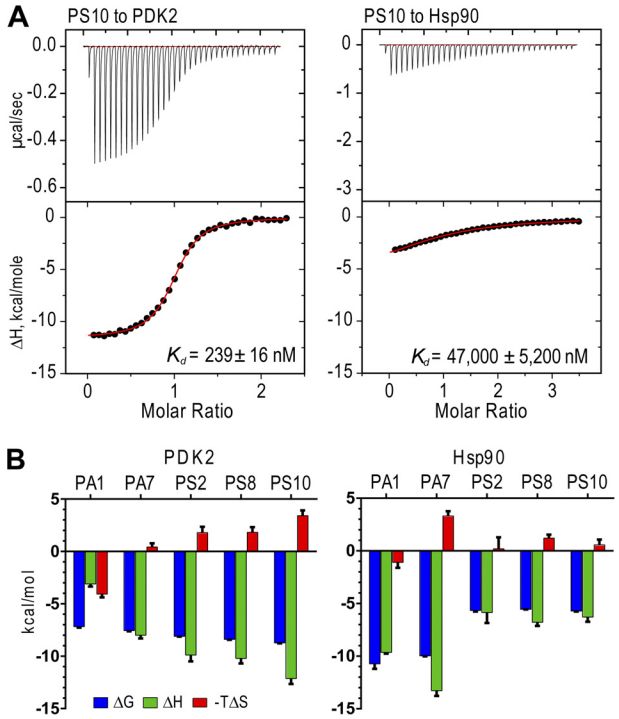

FIGURE 4. **Thermodynamic analysis of inhibitor binding to PDK2 and Hsp90.** *A*, thermograms of PS10 binding to PDK2 and Hsp90 obtained by ITC. *B*, thermodynamic signatures of inhibitor bindings to PDK2 (*left panel*) and Hsp90 (*right panel*); Δ*G*, Gibbs binding energy; Δ*H*, binding enthalpy; Δ*S*, binding entropy; *T*, absolute temperature.

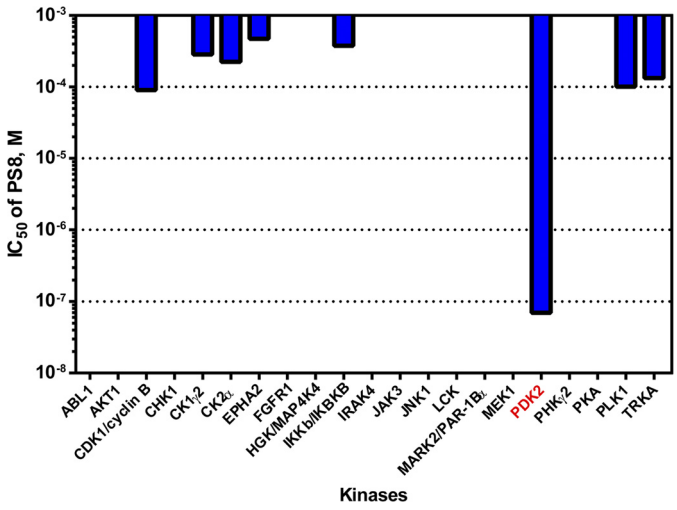

FIGURE 5. **Kinase profiling of compound PS8.** Inhibition of the 21 representative kinases, including PDK2, in the Human Kinome by PS8 were measured in the concentration range of 15 nM to 300 μM. IC_{50} values for each kinase were derived from individual inhibition curves. The IC_{50} for PDK2 is at least 3 orders of magnitude lower than the next lowest value for CDK1/cyclin B.

TABLE 3

IC_{50} value for the inhibition of the four PDK isoforms by PS8 and PS10

PDK activity was assayed with increasing concentrations (31.6 nM to 1 mM) of the inhibitor in the presence or absence of the E2/E3BP core of PDC as described under "Experimental Procedures." IC_{50} values were obtained by the curve fitting of inhibition isotherms using program Prism 6 (GraphPad Software, Inc.).

	IC_{50} of PS8		IC_{50} of PS10,
	− E2/E3BP	+ E2/E3BP	− E2/E3BP
	μM		μM
PDK1	2.50 ± 0.14	2.14 ± 0.33	2.07
PDK2	1.07 ± 0.14	0.71 ± 0.14	0.80
PDK3	13.72 ± 2.08	2.55 ± 0.38	21.30
PDK4	1.10 ± 0.21	0.84 ± 0.08	0.77

favorable (or more positive) (Fig. 4*B*, *left panel*). These gains in binding enthalpy indicate the progressively more favorable interactions between PDK2 and the inhibitors as PA1 is evolved into PS10, despite the accompanied relatively small entropic penalties (40). In contrast, the conversion from carbonyl group-containing compounds (PA1 and PA7) to the sulfonyl group-harboring counterparts (PS2, PS8, and PS10) results in significant losses of binding enthalpies for Hsp90 (Fig. 3*B*, *right panel*). The favorable binding enthalpies further support the vastly improved selectivity of PS8 and PS10 as PDK inhibitors over the parental compound PA1.

PS Series Inhibitors Show High Selectivity for PDK Isoforms—The selectivity of PS8 was studied by determining IC_{50} for the inhibition of a 21-kinase panel, including PDK2. PS8 shows the lowest IC_{50} of 70 nM for PDK2 under the assay conditions with myelin-binding protein as an artificial substrate (Fig. 5). All other kinases on the panel show at least 3 orders of magnitude higher IC_{50} values for inhibition by PS8. The results established the specificity for PS8 as a PDK2 inhibitor. To dissect the specificity of PS series inhibitors against the four PDK isoforms, *in vitro* kinase assays were performed with or without the E2/E3BP core of PDC. The E3 component is not included in the assay mixture, because E3 is not required for our kinase activity assay that measures incorporation of the ^{32}P-phosphoryl group into the E1 protein. PS8 inhibits all four isoforms at the submicromolar to the low micromolar range (Table 3). Except PDK4, PDK isoforms anchor to the E2/E3BP of PDC for optimal kinase activity *in vivo*. In the presence of E2/E3BP, PS8 is a more effective inhibitor for all PDK isoforms than in the absence of E2/E3BP, particularly for PDK3. The most improved IC_{50} value for PDK3 in the presence of E2/E3BP among the four PDK isoforms may be explained by the markedly reduced affinity of PDK3 for ATP/ADP, when this PDK isoform is bound to the PDC core (29). PS10 shows the similar IC_{50} values for the inhibition of four PDK isoforms when assayed in the absence of E2/E3BP (Table 3). The above results, taken together, indicate that both PS8 and PS10 are pan-PDK inhibitors.

To assess possible toxicity of PS series compounds due to nonspecific interactions, HeLa and HBEC30 cells were titrated with PS8. The IC_{50} values for the growth inhibition of HeLa and HBEC30 cells by PS8 are 223 and 253 μM, respectively. The toxicity of PS8 is 100-fold less potent than cycloheximide in both cell lines. Similarly, PS10 shows an IC_{50} of 284 μM for the growth inhibition of HeLa cells. These results suggest that the toxicity of PS8 and PS10 is minimal *in vivo*.

Pharmacokinetic Properties of PS8 and PS10—PS8 and PS10 both show half-lives of greater than 240 min *in vitro* in hepatic S9 fractions (data not shown), which suggest that neither is extensively metabolized by phase I oxidative or reductive metabolism. *In vivo*, both compounds show a rapid distribution phase, followed by a slower terminal elimination phase after i.p. delivery. The pharmacokinetic parameters on Table 4 show that the distribution and elimination of PS8 was slightly more rapid than PS10, possibly due to its somewhat more hydrophobic nature. Both compounds show good plasma exposure

(AUC_{last}) as well as a volume of distribution, which is suggestive of modest tissue penetration (Table 4).

PS10 Stimulates PDC Activity in Tissues of DIO Mice—Both PS8 and PS10 show good IC_{50} values for the four PDK isoforms (Table 3); however, PS10 was chosen for *in vivo* studies because of its better solubility in DMSO used in the formulation. Male C57BL/6J mice were fed a high fat diet for 3 weeks to produce a DIO model with impaired glucose tolerance. These DIO mice were initially treated with a single dose of either vehicle or PS10 (70 mg/kg) by i.p. injection. The animals were sacrificed 10 h later in the early morning in the fed state. Maximal enhancement of PDC activity by PS10 in tissues was achieved under these conditions. Tissues (heart, liver, kidneys, and quadriceps muscle) were harvested and analyzed for PDC activity by the radiochemical assay with [1-^{14}C]pyruvate as a substrate. Fig. 6*A* (*top*) shows that PDC activity was low in the heart and liver from vehicle-treated DIO mice. PS10 treatments result in 11- and 23-fold higher PDC activity in heart and liver, respectively, than the vehicle-treated. There is a 1.4-fold enhancement of PDC activity in PS10-treated kidneys compared with vehicle-treated. In contrast, there is no difference of PDC activity in quadriceps muscle between PS10-treated and vehicle-treated DIO mice. The elevated PDC activity correlates with significantly decreased amounts of the phosphorylated E1α subunit in heart and liver of PS10-treated DIO mice compared with vehicle-treated (Fig. 6*A*, *bottom*). These results corroborate that PS10 functions as a PDK inhibitor *in vivo* to attenuate phosphorylation levels of the E1α subunit, leading to stimulated PDC activity in DIO mice. The increased PDC activity is not due to enhanced phosphatase activity, because PS10 at up to 1 mM is

TABLE 4

Pharmacokinetic parameters for PS8 and PS10

Terminal $t_{½}$ indicates half-life of the terminal phase; C_{max} indicates observed maximum plasma concentration; t_{max} indicates time to reach C_{max}; AUC_{last} indicates area under the concentration-time curve from 0 to the last measured point; V_z/F indicates apparent volume of distribution during terminal phase; and *CL/F* indicates volume of plasma cleared of the drug per unit time, where *F* is the fraction bioavailable as compared to an i.v. dose, which is not known.

	PS8	PS10
Dose	20 mg/kg i.p.	70 mg/kg i.p.
Terminal $t_{½}$	93.3 min	161 min
C_{max}	7600 ng/ml	32,400 ng/ml
t_{max}	10 min	10 min
AUC_{last}	310,035 min ng/ml	1,905,136 min ng/ml
V_z/F	209 ml	172 ml
CL/F	1.55 ml/min	0.741 ml/min

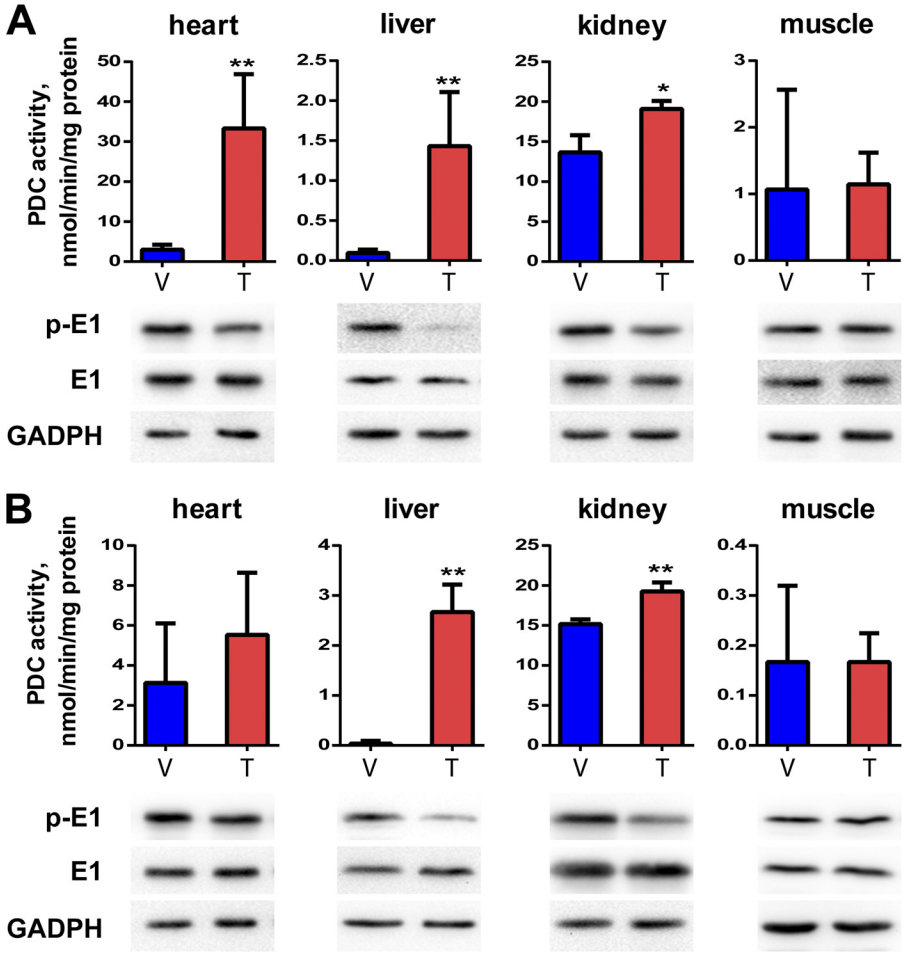

FIGURE 6. **Enhanced PDC activity with reduced phosphorylation level in PS10-treated DIO mice.** *A,* short term response. C57BL/6J male mice were fed a high fat diet for 3 weeks and treated with vehicle (*V*, $n = 4$) or PS10 at 70 mg/kg (*T*, $n = 4$) by a single i.p. injection while they had free access to food. Animals were sacrificed at 10 a.m., *i.e.* 10 h after the injection. Tissues were harvested and analyzed for PDC activity and phosphorylation levels of the E1α subunit. *Upper panel*, PDC activity in heart, liver, kidney, and muscle. *Lower panel*, amounts of the phosphorylated (*p-E1*) and total (*E1*) E1α subunit in different tissues determined by Western blotting analysis. *B,* long term response. C57BL/6J male mice were fed a high fat diet for 10 weeks and then treated with vehicle ($n = 3$) or PS10 at 70 mg/kg/day ($n = 3$) for 3 days. The remaining procedures and result presentation are as in *A*. **, $p < 0.01$; *, $p < 0.05$.

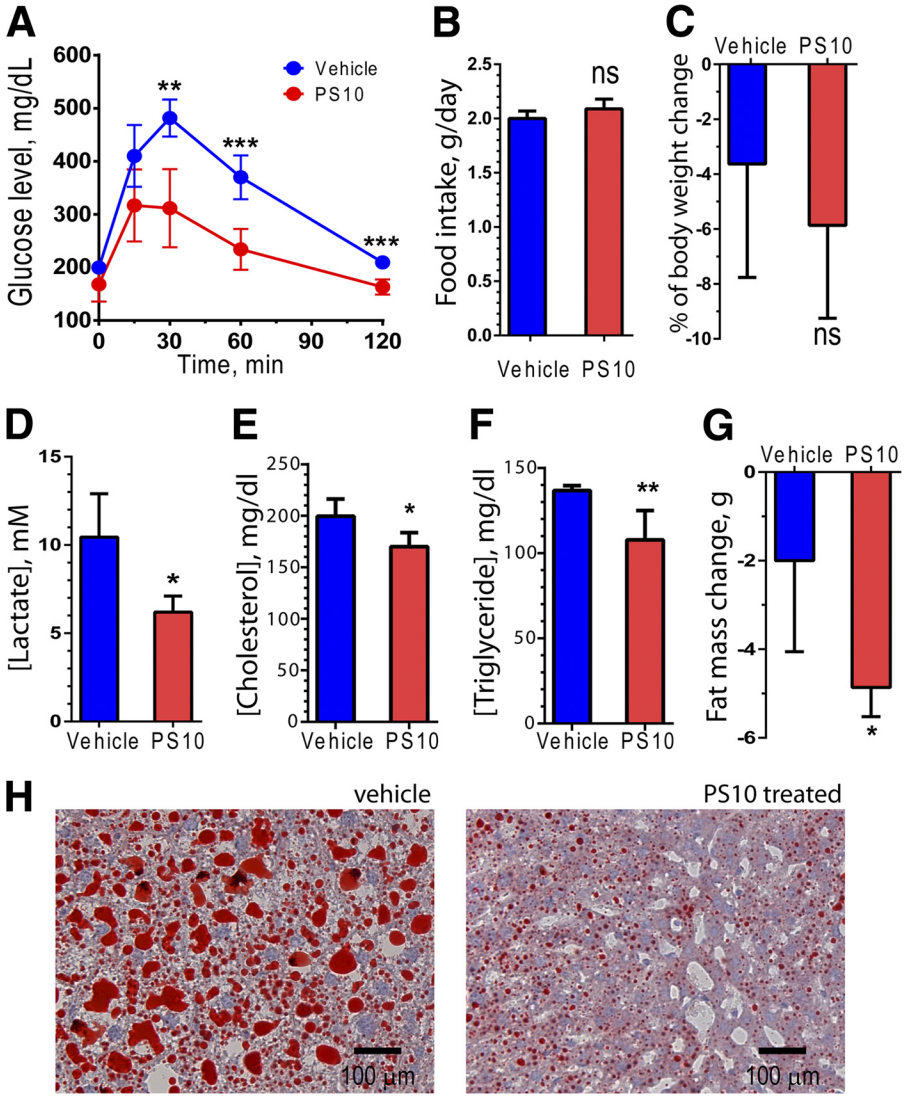

FIGURE 7. **Glucose- and lipid-controlling properties of PS10.** *A,* glucose tolerance test. C57BL/6J male mice were fed a high fat diet for 10 weeks and treated with vehicle ($n = 4$) or PS10 at 70 mg/kg/day ($n = 6$) for 4 weeks and were fasted for 6 h followed by injection of 1.5 g of glucose/kg by i.p. injection. Blood glucose levels were monitored at 0–2 h after the glucose injection. *B,* food intake of DIO mice fed the high fat diet for 10 weeks followed by treatments with vehicle ($n = 5$) or PS10 at 70 mg/kg/day ($n = 5$) for 1 week. *C,* body weight change in DIO mice from *A* after 6 weeks of treatment with vehicle or PS10. *D,* plasma lactate under the "Experimental Procedures." *E,* plasma cholesterol concentration in DIO mice from *C*. *F,* plasma triglycerides concentrations in DIO mice also from *C*. *G,* change in the fat mass. DIO mice were treated as in *B*. Fat mass was determined as described under "Experimental Procedures." *H,* Oil Red O stains of liver slices from vehicle- and PS10-treated DIO mice as in *B*. ***, $p < 0.001$; **, $p < 0.01$; *, $p < 0.05$; *ns*, not significant statistically.

without effect on PDP1 activity *in vitro*. In the next series of experiments, DIO mice were treated with vehicle or PS10 (70 mg/kg/day) for 3 days, and tissues were collected for biochemical studies. As shown in Fig. 6*B*, except in the heart, PDC activity profiles and the phospho-E1α subunit level are similar between the single-dose and multiple-dose treatments of DIO mice with PS10. In the heart, the prolonged PS10 treatment appears to attenuate the enhancement of PDK activity compared with the single administration of the compound.

PS10 Increases Glucose Tolerance and Lessens Hepatic Steatosis in DIO Mice—DIO mice on a high fat diet for 10 weeks were treated with vehicle or PS10 (70 mg/kg/day) by i.p. injections for 4 additional weeks and subjected to a glucose tolerance test. The vehicle and PS10 treatments were continued for 2 more days, and animals were sacrificed in the early morning while in the fed state, and tissues and blood were collected for biochemical studies. Results from the glucose tolerance tests (Fig. 7*A*) show that when challenged with 1.5 g/kg glucose, the plasma glucose level in the vehicle-treated control was at 200 mg/dl at 0 min, peaked at 482 mg/dl at 30 min, and reduced to 210 mg/dl at 120 min. In PS10-treated DIO mice, the glucose level at 168 mg/dl at 0 min was lower than that in vehicle-treated animals, reached 312 mg/dl at 30 min, and returned to 163 mg/dl at 120 min. The two groups of animals show significant differences in the glucose levels at 30, 60, and 120 min, with lower glucose levels uniformly observed in the PS10-treated DIO mice. The data therefore suggest that the PS10 treatment increases glucose tolerance over vehicle-treated DIO mice. Notably, there are no significant differences in food intake (Fig. 7*B*) and body weight (Fig. 7*C*) between the vehicle- and PS10-treated animals. DIO mice treated with PS10 also

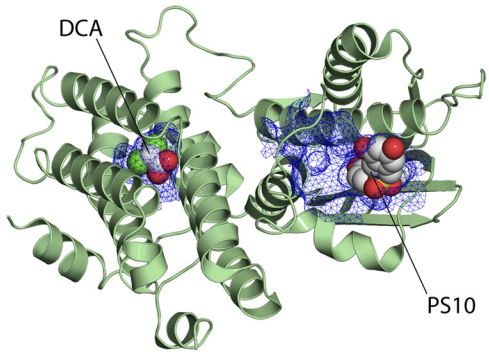

FIGURE 8. **Calculated volumes of the DCA-binding and ATP-binding pockets in PDK2.** The N-terminal domain of the PDK2 monomer with the allosteric site occupied by DCA is derived from coordinates of PDB code 2BU8. PDK inhibitor PS10 was modeled into the ATP-binding pocket in the C-terminal domain of the same monomer, according to the PS10 coordinates of PDB code 4MPN from this study. The volumes of the DCA-binding (211 Å^3) and ATP-binding (865 Å^3) pockets, as represented by *blue mesh*, were computed using program CASTp (50).

showed significantly lower plasma lactate (Fig. 7*D*), cholesterol (Fig. 7*E*), and triglyceride (Fig. 7*F*) levels and a reduction in fat mass (Fig. 7*G*), compared with the mice treated with vehicle. Moreover, larger amounts of fat were present in the liver of the vehicle-treated DIO mice compared with PS10-treated when the liver slices were stained with Oil Red O (Fig. 7*H*). The accumulated hepatic fat was primarily macrovesicular in vehicle-treated DIO mice and became microvesicular in the PS10-treated counterpart.

DISCUSSION

With the increased understanding that PDKs play a pivotal role in controlling glucose oxidation in disease states such as diabetes (3–5), cancer (8, 9, 11–14), and congestive heart failure, there is growing need for effective PDK inhibitors. The classic PDK inhibitor DCA binds to an enclosed allosteric site in the N-terminal domain, which is the binding site of PDC's substrate pyruvate for the physiological feedback inhibition (16, 17). However, this allosteric site is relatively small (volume = 211 Å^3), is also buried, and can only accommodate small ligands such as pyruvate and DCA (Fig. 8). The space limitation in the PDK allosteric site precludes the structure-based modification of DCA to improve its potency as a PDK inhibitor. The strategy of developing PDK inhibitors by targeting the lipoyl-binding pocket was unsuccessful *in vivo* (24). PDK2 and PDK3 are anchored to lipoyl-bearing domains on the E2/E3BP core of PDC for optimal kinase activity (29, 41). Dihydrolipoamide mimetics attenuate PDK2 and PDK3 activities by impeding binding of these PDK isoforms to the inner lipoyl-bearing domain of the E3/E3BP core (42). However, PDK4, which is up-regulated in obesity and diabetes (3–5), shows robust kinase activity without binding to the inner lipoyl-bearing domain of the E2/E3BP core. The binding of the dihydrolipoamide mimetic AZD7545 to PDK4 stimulates rather than inhibits its kinase activity considerably (26).

In this study, we undertook a different approach to develop a new generation of PDK inhibitors that dock to the ATP-binding pocket (volume = 865 Å^3) of PDK2, which is open and four times larger than the allosteric DCA-binding pocket (Fig. 8). The conservation in the ATP-binding pocket between Hsp90 and PDK2, both belonging to the GHKL ATPase/kinase superfamily (27), makes it possible to utilize the chemical scaffold in Hsp90 inhibitors PA1 and PA7 as the starting point for designing the PDK-specific inhibitors. The distinct conformations of the bound PA7 between the Hsp90-PA7 and PDK2-PA7 structures (Fig. 2*D*) provided the first clue for utilizing structure-based design to develop PDK-specific inhibitors. It is remarkable that a single replacement of the carbonyl group in PA7 with a sulfonyl group in PS2 results in a drastic conversion of an Hsp90 inhibitor (PA7) to a PDK inhibitor (PS2). Our results epitomize the feasibility of designing a highly selective kinase inhibitor by taking advantage of the unique structural features in the ATP-binding pocket.

The *in vivo* efficacy of the PDK inhibitor PS10 was evaluated in DIO mice. DIO mice fed a high fat diet develop symptoms characteristic of the metabolic syndrome, and if left on the diet long enough, the mice will eventually develop type 2 diabetes (43). The modest selectivity of PS10 for the four PDK isoforms is desirable, because PDK2/PDK4 double knock-out mice showed far more robust improvement in glucose tolerance and insulin sensitivity than the single PDK2 or PDK4 knock-out mice (7). PDC activity is low in the heart and liver from DIO mice fed a high fat diet for 3 weeks (Fig. 6, *A* and *B*). The effectiveness of PS10 as a PDK inhibitor *in vivo* is established by higher PDC activity in most tissues from PS10-treated over vehicle-treated DIO mice. The stimulation of PDC activity in the liver and heart is compelling, given that PS10 is competitive with ATP, which is usually present at 1–10 mM in the mitochondrial matrix (44, 45). The results may be explained by the accumulation of PS10 in the mitochondrial matrix. It is equally plausible that the modest inhibition of PDKs by PS10 *in vivo* is sufficient to tip the balance between PDKs and PDPs in favor of the latter, resulting in the significant dephosphorylation of PDC.

The increased PDC flux in liver promotes glucose disposal, leading to improved glucose tolerance in PS10-treated DIO mice (Fig. 7*A*). The reduced plasma level of the gluconeogenic substrate lactate (Fig. 7*D*) explains in part the lower glucose concentrations in PS10-treated DIO mice (Fig. 7*A*). In the heart, a single dose of PS10 treatment results in drastic enhancement of PDC activity (Fig. 6*A*); however, the prolonged PS10 treatment causes a reduction in the fold increase of PDC activity (Fig. 6*B*). The results suggest a reset of the cardiac PDC flux during the long term PS10 dosing. PDK4 expression is up-regulated in right ventricular hypertrophy causing an increase in glycolysis over glucose oxidation (46). The increased cardiac PDC flux by PS10 may offer an approach to mitigating impaired glucose oxidation in congenital heart failure.

The above increased glucose disposal through enhanced PDC flux is coupled with decreased lipogenesis in PS10-treated DIO mice, as demonstrated by the lessened hepatic steatosis, lower fat mass, and attenuated plasma cholesterol as well as triglyceride levels (Fig. 7, *D–H*). The combination of reduced lipogenesis and increased glucose oxidation has been reported in acetyl-CoA carboxylase 2 (47) or PDK4 (48) knock-out mice on high fat diets. In the liver of PDK4-deficient mice, the expression of both fatty-acid synthase and acetyl-CoA carboxylase is reduced, which likely results in reduced lipogenesis with

improved hepatic steatosis (43). Interestingly, the two transcription factors that promote fatty acid oxidation, *i.e.* peroxisome proliferator-activated receptor α and PGC-1α (49) in PDK4-deficient mice fed the high fat diet are restored to the levels of the wild-type animals on chow diet (48). The excess acetyl-CoA from both glucose and fatty acid oxidation is converted to ketone bodies, because plasma concentrations of both β-hydroxybutyrate and acetoacetate were considerably elevated in PDK2/PDK4 double knock-out mice compared with the wild type (7). Taken together, the present results illustrate the therapeutic potentials of PDK inhibitors in increasing hepatic glucose oxidation through PDC flux while suppressing lipogenesis in the liver of diet-induced obesity.

Acknowledgments—Crystal structures presented in this report are derived from work performed at Argonne National Laboratory, Structural Biology Center at the Advanced Photon Source, operated under Department of Energy Contract DE-AC02-06CH11357.

REFERENCES

1. Reed, L. J. (2001) A trail of research from lipoic acid to α-keto acid dehydrogenase complexes. *J. Biol. Chem.* **276,** 38329–38336
2. Randle, P. J. (1995) Metabolic fuel selection: general integration at the whole-body level. *Proc. Nutr. Soc.* **54,** 317–327
3. Harris, R. A., Hawes, J. W., Popov, K. M., Zhao, Y., Shimomura, Y., Sato, J., Jaskiewicz, J., and Hurley, T. D. (1997) Studies on the regulation of the mitochondrial α-ketoacid dehydrogenase complexes and their kinases. *Adv. Enzyme Regul.* **37,** 271–293
4. Wu, P., Inskeep, K., Bowker-Kinley, M. M., Popov, K. M., and Harris, R. A. (1999) Mechanism responsible for inactivation of skeletal muscle pyruvate dehydrogenase complex in starvation and diabetes. *Diabetes* **48,** 1593–1599
5. Rosa, G., Di Rocco, P., Manco, M., Greco, A. V., Castagneto, M., Vidal, H., and Mingrone, G. (2003) Reduced PDK4 expression associates with increased insulin sensitivity in postobese patients. *Obes. Res.* **11,** 176–182
6. Kuzuya, T., Katano, Y., Nakano, I., Hirooka, Y., Itoh, A., Ishigami, M., Hayashi, K., Honda, T., Goto, H., Fujita, Y., Shikano, R., Muramatsu, Y., Bajotto, G., Tamura, T., Tamura, N., and Shimomura, Y. (2008) Regulation of branched-chain amino acid catabolism in rat models for spontaneous type 2 diabetes mellitus. *Biochem. Biophys. Res. Commun.* **373,** 94–98
7. Jeoung, N. H., Rahimi, Y., Wu, P., Lee, W. N., and Harris, R. A. (2012) Fasting induces ketoacidosis and hypothermia in PDHK2/PDHK4-double-knockout mice. *Biochem. J.* **443,** 829–839
8. Papandreou, I., Cairns, R. A., Fontana, L., Lim, A. L., and Denko, N. C. (2006) HIF-1 mediates adaptation to hypoxia by actively downregulating mitochondrial oxygen consumption. *Cell Metab.* **3,** 187–197
9. Kim, J. W., Tchernyshyov, I., Semenza, G. L., and Dang, C. V. (2006) HIF-1-mediated expression of pyruvate dehydrogenase kinase: a metabolic switch required for cellular adaptation to hypoxia. *Cell Metab.* **3,** 177–185
10. Kaplon, J., Zheng, L., Meissl, K., Chaneton, B., Selivanov, V. A., Mackay, G., van der Burg, S. H., Verdegaal, E. M., Cascante, M., Shlomi, T., Gottlieb, E., and Peeper, D. S. (2013) A key role for mitochondrial gatekeeper pyruvate dehydrogenase in oncogene-induced senescence. *Nature* **498,** 109–112
11. Michelakis, E. D., Sutendra, G., Dromparis, P., Webster, L., Haromy, A., Niven, E., Maguire, C., Gammer, T. L., Mackey, J. R., Fulton, D., Abdulkarim, B., McMurtry, M. S., and Petruk, K. C. (2010) Metabolic modulation of glioblastoma with dichloroacetate. *Sci. Transl. Med.* **2,** 31ra34
12. Lu, C. W., Lin, S. C., Chen, K. F., Lai, Y. Y., and Tsai, S. J. (2008) Induction of pyruvate dehydrogenase kinase-3 by hypoxia-inducible factor-1 promotes metabolic switch and drug resistance. *J. Biol. Chem.* **283,** 28106–28114
13. Hitosugi, T., Fan, J., Chung, T. W., Lythgoe, K., Wang, X., Xie, J., Ge, Q., Gu, T. L., Polakiewicz, R. D., Roesel, J. L., Chen, G. Z., Boggon, T. J., Lonial, S., Fu, H., Khuri, F. R., Kang, S., and Chen, J. (2011) Tyrosine phosphorylation of mitochondrial pyruvate dehydrogenase kinase 1 is important for cancer metabolism. *Mol. Cell* **44,** 864–877
14. Bonnet, S., Archer, S. L., Allalunis-Turner, J., Haromy, A., Beaulieu, C., Thompson, R., Lee, C. T., Lopaschuk, G. D., Puttagunta, L., Bonnet, S., Harry, G., Hashimoto, K., Porter, C. J., Andrade, M. A., Thebaud, B., and Michelakis, E. D. (2007) A mitochondria-K^+ channel axis is suppressed in cancer and its normalization promotes apoptosis and inhibits cancer growth. *Cancer Cell* **11,** 37–51
15. Whitehouse, S., and Randle, P. J. (1973) Activation of pyruvate dehydrogenase in perfused rat heart by dichloroacetate (Short Communication). *Biochem. J.* **134,** 651–653
16. Kato, M., Li, J., Chuang, J. L., and Chuang, D. T. (2007) Distinct structural mechanisms for inhibition of pyruvate dehydrogenase kinase isoforms by AZD7545, dichloroacetate, and radicicol. *Structure* **15,** 992–1004
17. Knoechel, T. R., Tucker, A. D., Robinson, C. M., Phillips, C., Taylor, W., Bungay, P. J., Kasten, S. A., Roche, T. E., and Brown, D. G. (2006) Regulatory roles of the N-terminal domain based on crystal structures of human pyruvate dehydrogenase kinase 2 containing physiological and synthetic ligands. *Biochemistry* **45,** 402–415
18. Jiang, D. K., Sun, J., Cao, G., Liu, Y., Lin, D., Gao, Y. Z., Ren, W. H., Long, X. D., Zhang, H., Ma, X. P., Wang, Z., Jiang, W., Chen, T. Y., Gao, Y., Sun, L. D., Long, J. R., Huang, H. X., Wang, D., Yu, H., Zhang, P., Tang, L. S., Peng, B., Cai, H., Liu, T. T., Zhou, P., Liu, F., Lin, X., Tao, S., Wan, B., Sai-Yin, H. X., Qin, L. X., Yin, J., Liu, L., Wu, C., Pei, Y., Zhou, Y. F., Zhai, Y., Lu, P. X., Tan, A., Zuo, X. B., Fan, J., Chang, J., Gu, X., Wang, N. J., Li, Y., Liu, Y. K., Zhai, K., Zhang, H., Hu, Z., Liu, J., Yi, Q., Xiang, Y., Shi, R., Ding, Q., Zheng, W., Shu, X. O., Mo, Z., Shugart, Y. Y., Zhang, X. J., Zhou, G., Shen, H., Zheng, S. L., Xu, J., and Yu, L. (2013) Genetic variants in STAT4 and HLA-DQ genes confer risk of hepatitis B virus-related hepatocellular carcinoma. *Nat. Genet.* **45,** 72–75
19. Stacpoole, P. W., Barnes, C. L., Hurbanis, M. D., Cannon, S. L., and Kerr, D. S. (1997) Treatment of congenital lactic acidosis with dichloroacetate. *Arch. Dis. Child.* **77,** 535–541
20. Korotchkina, L. G., Sidhu, S., and Patel, M. S. (2004) R-lipoic acid inhibits mammalian pyruvate dehydrogenase kinase. *Free Radic. Res.* **38,** 1083–1092
21. Ferriero, R., Manco, G., Lamantea, E., Nusco, E., Ferrante, M. I., Sordino, P., Stacpoole, P. W., Lee, B., Zeviani, M., and Brunetti-Pierri, N. (2013) Phenylbutyrate therapy for pyruvate dehydrogenase complex deficiency and lactic acidosis. *Sci. Transl. Med.* **5,** 175ra31
22. Iannitti, T., and Palmieri, B. (2011) Clinical and experimental applications of sodium phenylbutyrate. *Drugs R D* **11,** 227–249
23. Mayers, R. M., Butlin, R. J., Kilgour, E., Leighton, B., Martin, D., Myatt, J., Orme, J. P., and Holloway, B. R. (2003) AZD7545, a novel inhibitor of pyruvate dehydrogenase kinase 2 (PDHK2), activates pyruvate dehydrogenase *in vivo* and improves blood glucose control in obese (fa/fa) Zucker rats. *Biochem. Soc. Trans.* **31,** 1165–1167
24. Aicher, T. D., Anderson, R. C., Gao, J., Shetty, S. S., Coppola, G. M., Stanton, J. L., Knorr, D. C., Sperbeck, D. M., Brand, L. J., Vinluan, C. C., Kaplan, E. L., Dragland, C. J., Tomaselli, H. C., Islam, A., Lozito, R. J., Liu, X., Maniara, W. M., Fillers, W. S., DelGrande, D., Walter, R. E., and Mann, W. R. (2000) Secondary amides of (*R*)-3,3,3-trifluoro-2-hydroxy-2-methylpropionic acid as inhibitors of pyruvate dehydrogenase kinase. *J. Med. Chem.* **43,** 236–249
25. Kato, M., Wynn, R. M., Chuang, J. L., Tso, S. C., Machius, M., Li, J., and Chuang, D. T. (2008) Structural basis for inactivation of the human pyruvate dehydrogenase complex by phosphorylation: role of disordered phosphorylation loops. *Structure* **16,** 1849–1859
26. Wynn, R. M., Kato, M., Chuang, J. L., Tso, S. C., Li, J., and Chuang, D. T. (2008) Pyruvate dehydrogenase kinase-4 structures reveal a metastable open conformation fostering robust core-free basal activity. *J. Biol. Chem.* **283,** 25305–25315
27. Dutta, R., and Inouye, M. (2000) GHKL, an emergent ATPase/kinase superfamily. *Trends Biochem. Sci.* **25,** 24–28
28. Steussy, C. N., Popov, K. M., Bowker-Kinley, M. M., Sloan, R. B., Jr., Harris,

R. A., and Hamilton, J. A. (2001) Structure of pyruvate dehydrogenase kinase. Novel folding pattern for a serine protein kinase. *J. Biol. Chem.* **276,** 37443–37450
29. Kato, M., Chuang, J. L., Tso, S. C., Wynn, R. M., and Chuang, D. T. (2005) Crystal structure of pyruvate dehydrogenase kinase 3 bound to lipoyl domain 2 of human pyruvate dehydrogenase complex. *EMBO J.* **24,** 1763–1774
30. Kung, P. P., Huang, B., Zhang, G., Zhou, J. Z., Wang, J., Digits, J. A., Skaptason, J., Yamazaki, S., Neul, D., Zientek, M., Elleraas, J., Mehta, P., Yin, M. J., Hickey, M. J., Gajiwala, K. S., Rodgers, C., Davies, J. F., and Gehring, M. R. (2010) Dihydroxyphenylisoindoline amides as orally bioavailable inhibitors of the heat shock protein 90 (hsp90) molecular chaperone. *J. Med. Chem.* **53,** 499–503
31. Murray, C. W., Carr, M. G., Callaghan, O., Chessari, G., Congreve, M., Cowan, S., Coyle, J. E., Downham, R., Figueroa, E., Frederickson, M., Graham, B., McMenamin, R., O'Brien, M. A., Patel, S., Phillips, T. R., Williams, G., Woodhead, A. J., and Woolford, A. J. (2010) Fragment-based drug discovery applied to Hsp90. Discovery of two lead series with high ligand efficiency. *J. Med. Chem.* **53,** 5942–5955
32. Keller, S., Vargas, C., Zhao, H., Piszczek, G., Brautigam, C. A., and Schuck, P. (2012) High precision isothermal titration calorimetry with automated peak-shape analysis. *Anal. Chem.* **84,** 5066–5073
33. Tso, S. C., Qi, X., Gui, W. J., Chuang, J. L., Morlock, L. K., Wallace, A. L., Ahmed, K., Laxman, S., Campeau, P. M., Lee, B. H., Hutson, S. M., Tu, B. P., Williams, N. S., Tambar, U. K., Wynn, R. M., and Chuang, D. T. (2013) Structure-based design and mechanisms of allosteric inhibitors for mitochondrial branched-chain α-ketoacid dehydrogenase kinase. *Proc. Natl. Acad. Sci. U.S.A.* **110,** 9728–9733
34. Li, J., Kato, M., and Chuang, D. T. (2009) Pivotal role of the C-terminal DW-motif in mediating inhibition of pyruvate dehydrogenase kinase 2 by dichloroacetate. *J. Biol. Chem.* **284,** 34458–34467
35. Kukimoto-Niino, M., Tokmakov, A., Terada, T., Ohbayashi, N., Fujimoto, T., Gomi, S., Shiromizu, I., Kawamoto, M., Matsusue, T., Shirouzu, M., and Yokoyama, S. (2011) Inhibitor-bound structures of human pyruvate dehydrogenase kinase 4. *Acta Crystallogr. D Biol. Crystallogr.* **67,** 763–773
36. Dymock, B. W., Barril, X., Brough, P. A., Cansfield, J. E., Massey, A., McDonald, E., Hubbard, R. E., Surgenor, A., Roughley, S. D., Webb, P., Workman, P., Wright, L., and Drysdale, M. J. (2005) Novel, potent small-molecule inhibitors of the molecular chaperone Hsp90 discovered through structure-based design. *J. Med. Chem.* **48,** 4212–4215
37. Feldman, R. I., Mintzer, B., Zhu, D., Wu, J. M., Biroc, S. L., Yuan, S., Emayan, K., Chang, Z., Chen, D., Arnaiz, D. O., Bryant, J., Ge, X. S., Whitlow, M., Adler, M., Polokoff, M. A., Li, W. W., Ferrer, M., Sato, T., Gu, J. M., Shen, J., Tseng, J. L., Dinter, H., and Buckman, B. (2009) Potent triazolothione inhibitor of heat-shock protein-90. *Chem. Biol. Drug Des.* **74,** 43–50
38. Hiromasa, Y., and Roche, T. E. (2008) Critical role of specific ions for ligand-induced changes regulating pyruvate dehydrogenase kinase isoform 2. *Biochemistry* **47,** 2298–2311
39. Green, T., Grigorian, A., Klyuyeva, A., Tuganova, A., Luo, M., and Popov, K. M. (2008) Structural and functional insights into the molecular mechanisms responsible for the regulation of pyruvate dehydrogenase kinase 2. *J. Biol. Chem.* **283,** 15789–15798
40. Freire, E. (2008) Do enthalpy and entropy distinguish first in class from best in class? *Drug Discov. Today* **13,** 869–874
41. Baker, J. C., Yan, X., Peng, T., Kasten, S., and Roche, T. E. (2000) Marked differences between two isoforms of human pyruvate dehydrogenase kinase. *J. Biol. Chem.* **275,** 15773–15781
42. Tuganova, A., Klyuyeva, A., and Popov, K. M. (2007) Recognition of the inner lipoyl-bearing domain of dihydrolipoyl transacetylase and of the blood glucose-lowering compound AZD7545 by pyruvate dehydrogenase kinase 2. *Biochemistry* **46,** 8592–8602
43. Wang, C. Y., and Liao, J. K. (2012) A mouse model of diet-induced obesity and insulin resistance. *Methods Mol. Biol.* **821,** 421–433
44. Kennedy, H. J., Pouli, A. E., Ainscow, E. K., Jouaville, L. S., Rizzuto, R., and Rutter, G. A. (1999) Glucose generates sub-plasma membrane ATP microdomains in single islet beta-cells. Potential role for strategically located mitochondria. *J. Biol. Chem.* **274,** 13281–13291
45. Metelkin, E., Demin, O., Kovács, Z., and Chinopoulos, C. (2009) Modeling of ATP-ADP steady-state exchange rate mediated by the adenine nucleotide translocase in isolated mitochondria. *FEBS J.* **276,** 6942–6955
46. Piao, L., Sidhu, V. K., Fang, Y. H., Ryan, J. J., Parikh, K. S., Hong, Z., Toth, P. T., Morrow, E., Kutty, S., Lopaschuk, G. D., and Archer, S. L. (2013) FOXO1-mediated upregulation of pyruvate dehydrogenase kinase-4 (PDK4) decreases glucose oxidation and impairs right ventricular function in pulmonary hypertension: therapeutic benefits of dichloroacetate. *J. Mol. Med.* **91,** 333–346
47. Choi, C. S., Savage, D. B., Abu-Elheiga, L., Liu, Z. X., Kim, S., Kulkarni, A., Distefano, A., Hwang, Y. J., Reznick, R. M., Codella, R., Zhang, D., Cline, G. W., Wakil, S. J., and Shulman, G. I. (2007) Continuous fat oxidation in acetyl-CoA carboxylase 2 knockout mice increases total energy expenditure, reduces fat mass, and improves insulin sensitivity. *Proc. Natl. Acad. Sci. U.S.A.* **104,** 16480–16485
48. Hwang, B., Jeoung, N. H., and Harris, R. A. (2009) Pyruvate dehydrogenase kinase isoenzyme 4 (PDHK4) deficiency attenuates the long-term negative effects of a high saturated fat diet. *Biochem. J.* **423,** 243–252
49. Lin, J., Handschin, C., and Spiegelman, B. M. (2005) Metabolic control through the PGC-1 family of transcription coactivators. *Cell Metab.* **1,** 361–370
50. Dundas, J., Ouyang, Z., Tseng, J., Binkowski, A., Turpaz, Y., and Liang, J. (2006) CASTp: computed atlas of surface topography of proteins with structural and topographical mapping of functionally annotated residues. *Nucleic Acids Res.* **34,** W116–W118